

Implementation of Lees-Edwards periodic boundary conditions for direct numerical simulations of particle dispersions under shear flow

Hideki Kobayashi^{1,2, a)} and Ryoichi Yamamoto^{1,2, b)}

¹⁾*Department of Chemical Engineering, Kyoto University, Kyoto 615-8510, Japan*

²⁾*CREST Japan Science and Technology Agency, Kawaguchi 332-0012, Japan*

(Dated: 29 May 2018)

A general methodology is presented to perform direct numerical simulations of particle dispersions in a shear flow with Lees-Edwards periodic boundary conditions. The Navier-Stokes equation is solved in oblique coordinates to resolve the incompatibility of the fluid motions with the sheared geometry, and the force coupling between colloidal particles and the host fluid is imposed by using a smoothed profile method. The validity of the method is carefully examined by comparing the present numerical results with experimental viscosity data for particle dispersions in a wide range of volume fractions and shear rates including nonlinear shear-thinning regimes.

PACS numbers: 83.80.Rs, 47.57.Ng, 83.80.Hj, 83.10.Rs

Keywords: colloidal dispersion, simulation, hydrodynamic interaction, shear flow

^{a)}Electronic mail: hidekb@cheme.kyoto-u.ac.jp

^{b)}Electronic mail: ryoichi@cheme.kyoto-u.ac.jp

I. INTRODUCTION

Understanding the rheological properties of particle dispersions has been an important problem in many fields of science and engineering. When a dispersion is subjected to shear flow, the flow properties of the dispersion show a variety of non-Newtonian behaviors such as shear thinning and shear thickening. These non-Newtonian behaviors are associated with the changing microstructures of the dispersion, and several different physical mechanisms for these peculiar behaviors have been proposed.

In recent years, several numerical methods have been developed to accurately simulate particle dispersions, and they are all based on a similar approach, which involves resolving the fluid motion simultaneously with the particle motion. We refer to this approach as direct numerical simulation (DNS). Recently, we have developed a numerical method, which we call the smoothed profile method (SPM), for the DNS of particulate flows.¹⁻⁴ In the SPM, the Navier-Stokes equation for the fluid motion is discretized on a fixed grid, and the Newton's and Euler's equations for the particle motion are solved simultaneously with the fluid motion. One simple technique to impose shear flow with the DNS approach that maintains conventional cubic periodic boundary conditions is to apply a spatially periodic external force to generate a periodic flow profile. We have successfully used a zigzag flow profile to impose both steady and oscillatory shear flows in the DNS of spherical particle dispersions.^{3,4}

When a zero-wavevector shear flow is required, the usual cubic periodic boundary conditions must be modified to be compatible with a time-dependent shear deformation of the simulation cell. Such a modification was proposed by Lees and Edwards⁵ and is commonly used in various simulation studies. The Lees-Edwards boundary conditions can be very easily implemented for particle-based simulations such as molecular dynamics simulations. However, care must be taken to implement these conditions in continuum grid-based simulations such as computational fluid dynamics or time-dependent Ginzburg-Landau equations. The most useful implementation of the Lees-Edwards periodic boundary conditions for grid-based simulations is to solve the dynamic equations in deformed (oblique) coordinates.⁶⁻⁸ Onuki proposed a general methodology to examine the phase transition dynamics and rheology in the presence of shear flow,⁶ and it has been successfully used in several simulation studies and particularly for polymeric fluids in shear flow.⁹⁻¹²

The aim of this short paper is to propose a method to implement the Lees-Edwards periodic boundary conditions to simulate dispersions of solid particles in host fluids by the combinatory use of the SPM and the oblique coordinates.

II. METHOD

In the SPM, the boundary between the solid particles and the solvent is replaced with a continuous interface by assuming a smoothed profile. This simple modification enables us to calculate hydrodynamic interactions both efficiently and accurately without neglecting many-body interactions. The equation governing the dynamics of particle dispersion is a modified Navier-Stokes equation:

$$\rho \left\{ \frac{\partial \mathbf{u}}{\partial t} + (\mathbf{u} \cdot \nabla) \mathbf{u} \right\} = \nabla \cdot \boldsymbol{\sigma} + \rho \phi \mathbf{f}_p - K \rho (u_x - \dot{\gamma} y) \mathbf{e}_x \quad (1)$$

with the condition of incompressibility $\nabla \cdot \mathbf{u} = 0$, where ρ is the solvent density,

$$\boldsymbol{\sigma} = -p \mathbf{I} + \eta_f \{ \nabla \mathbf{u} + (\nabla \mathbf{u})^T \} \quad (2)$$

is the Newtonian stress tensor with a solvent viscosity of η_f , and $\mathbf{u}(\mathbf{r}, t)$ and $p(\mathbf{r}, t)$ are the velocity and pressure of the dispersion, respectively. A smoothed profile function $0 \leq \phi(\mathbf{r}, t) \leq 1$ distinguishes between the fluid and particle domains as well as yields $\phi = 1$ in the particle domain and $\phi = 0$ in the fluid domain. These domains are separated by thin interstitial regions with thicknesses characterized by ξ . The dispersion density ρ is represented as

$$\rho = (1 - \phi) \rho_f + \phi \rho_p \quad (3)$$

where ρ_f and ρ_p are the solvent and particle densities, respectively. Only neutral buoyancy dispersions with $\rho = \rho_f = \rho_p$ are simulated in the present study. The body force $\phi \mathbf{f}_p$ is introduced so that the total velocity field \mathbf{u} of the dispersion satisfies $\mathbf{u}(\mathbf{r}) = (1 - \phi) \mathbf{u}_f(\mathbf{r}) + \phi \mathbf{u}_p(\mathbf{r})$, where \mathbf{u}_f is the fluid velocity and \mathbf{u}_p represents the rigid motions of the particles. The incompressible condition $\nabla \cdot \mathbf{u}$ thus ensures $\nabla \phi \cdot (\mathbf{u}_p - \mathbf{u}_f)$ because both \mathbf{u}_f and \mathbf{u}_p satisfy incompressible conditions. The gradient of ϕ is proportional to the surface-normal vector and has a support on the interfacial domains. Therefore, the body force $\phi \mathbf{f}_p$ introduced to satisfy the rigidity of the particles ensure the appropriate impermeability boundary conditions at the fluid-particle interface, while the non-slip boundary conditions

are imposed automatically by the viscous stress term in the Navier-Stokes equation. More detailed explanations and the mathematical expressions for ϕ and $\phi \mathbf{f}_p$ were also detailed in our previous papers.^{1,2}

The last term in Eq.(1) represents the external force needed to maintain linear shear flow:

$$u_x = \dot{\gamma}y \quad (4)$$

where $\dot{\gamma}$ is the shear rate, and K is a constant that determines the amplitude of the external force. Here we impose only the zero-wavevector shear flow so that the averaged fluid velocity becomes compatible with Eq.(4).

The motion of the i -th particle in a dispersion is governed by Newton's and Euler's equations of motion:

$$M_i \frac{d}{dt} \mathbf{v}_i = \mathbf{f}_i^H + \mathbf{f}_i^P + \mathbf{g}_i^V, \quad \frac{d}{dt} \mathbf{r}_i = \mathbf{v}_i \quad (5)$$

$$\mathbf{I}_i \cdot \frac{d}{dt} \boldsymbol{\omega}_i = \mathbf{n}_i^H + \mathbf{g}_i^\omega \quad (6)$$

where \mathbf{r}_i , \mathbf{v}_i , and $\boldsymbol{\omega}_i$ are the position, translational velocity, and rotational velocity of the colloidal particles, respectively. M_i and \mathbf{I}_i are the mass and the moment of inertia, and \mathbf{f}_i^H and \mathbf{n}_i^H are the hydrodynamic force and torque exerted by the solvent on the colloidal particles, respectively^{1,2}. \mathbf{g}_i^V and \mathbf{g}_i^ω are the random force and torque, respectively, due to thermal fluctuations. The temperature of the system is defined such that the long-term diffusive motion of the colloidal particles reproduces the Stokes-Einstein rule.^{3,4} \mathbf{f}_i^P represents the potential force due to direct inter-particle interactions such as through the Coulombic and Lennard-Jones potentials.

Eqs.(1), (5), and (6) are solved simultaneously in the SPM. However, this task is not easy with an ordinary periodic boundary condition because Eq.(1) depends explicitly on y , which leads to a violation of the translational invariance. This problem can be eliminated by using oblique coordinates. Fig. 1 represents a schematic illustration of the present coordinate transform. At a time $t = t_0$, a spherical solid particle is located in a solvent in Fig. 1 (a) where the solvent is discretized into square grids in an ordinary rectangular coordinate system. In Fig. 1 (b), the grids are deformed due to the shear flow that is applied for $t > t_0$ while the shape of the solid particle is unchanged. The same situation is depicted in a transformed (oblique) frame in Fig. 1 (c) where the grid has not moved (i.e., it remains rectangular), but the shape of the solid particle changes over time due to the shear flow.

To formulate the oblique coordinate transformation based on tensor analysis, we began by redefining the covariant basis $\hat{\mathbf{E}}_i$ and contravariant basis $\hat{\mathbf{E}}^i$ in oblique coordinates rather than using the expressions shown in the literature.⁶⁻⁸ Fig. 2 provides a definition of the basis vectors. Using a rectangular unit vector, $\hat{\mathbf{E}}_i$ and $\hat{\mathbf{E}}^i$ are expressed as

$$\begin{aligned}\hat{\mathbf{E}}_1 &= \mathbf{e}_x & \hat{\mathbf{E}}^1 &= \mathbf{e}_x - \dot{\gamma}t\mathbf{e}_y \\ \hat{\mathbf{E}}_2 &= \dot{\gamma}t\mathbf{e}_x + \mathbf{e}_y & \hat{\mathbf{E}}^2 &= \mathbf{e}_y \\ \hat{\mathbf{E}}_3 &= \mathbf{e}_z & \hat{\mathbf{E}}^3 &= \mathbf{e}_z\end{aligned}\tag{7}$$

where \mathbf{e}_α is the unit vector in the $\alpha(=x, y, z)$ direction in the original rectangular coordinate system. We can obtain contravariant (covariant) vector components A^i (A_i) using $\mathbf{A} \cdot \hat{\mathbf{E}}^i$ ($\mathbf{A} \cdot \hat{\mathbf{E}}_i$). The positional vector $\mathbf{r} \equiv x\mathbf{e}_x + y\mathbf{e}_y + z\mathbf{e}_z$ is transformed from the rectangular coordinate expression \mathbf{r} to the oblique coordinate expression $\hat{\mathbf{r}}$ as follows:

$$\begin{aligned}\mathbf{r} &\equiv x\mathbf{e}_x + y\mathbf{e}_y + z\mathbf{e}_z \\ &= (\mathbf{r} \cdot \hat{\mathbf{E}}^1)\hat{\mathbf{E}}_1 + (\mathbf{r} \cdot \hat{\mathbf{E}}^2)\hat{\mathbf{E}}_2 + (\mathbf{r} \cdot \hat{\mathbf{E}}^3)\hat{\mathbf{E}}_3 \\ &= \hat{x}^1\hat{\mathbf{E}}_1 + \hat{x}^2\hat{\mathbf{E}}_2 + \hat{x}^3\hat{\mathbf{E}}_3 \equiv \hat{\mathbf{r}},\end{aligned}\tag{8}$$

where the contravariant components ($\hat{x}^1, \hat{x}^2, \hat{x}^3$) are expressed as

$$\begin{aligned}\hat{x}^1 &= x - \dot{\gamma}ty \\ \hat{x}^2 &= y \\ \hat{x}^3 &= z\end{aligned}\tag{9}$$

and the time in oblique coordinates is expressed as $\hat{t} = t$. Each contravariant component is transformed to a covariant component by using the metric tensors $G_{ij} = \hat{\mathbf{E}}_i \cdot \hat{\mathbf{E}}_j$ and $G^{ij} = \hat{\mathbf{E}}^i \cdot \hat{\mathbf{E}}^j$. Then, the transformation can be expressed as

$$A^i = G^{ij}A_j\tag{10}$$

$$A_i = G_{ij}A^j\tag{11}$$

The physical quantities in Eq. (1) are transformed as indicated below:

$$\hat{p}(\hat{\mathbf{r}}, \hat{t}) = p(\mathbf{r}, t)\tag{12}$$

$$\hat{\phi}(\hat{\mathbf{r}}, \hat{t}) = \phi(\mathbf{r}, t)\tag{13}$$

$$\hat{\mathbf{u}}(\hat{\mathbf{r}}, \hat{t}) = \mathbf{u}(\mathbf{r}, t) - \dot{\gamma}y\mathbf{e}_x\tag{14}$$

$$\hat{\phi}\hat{\mathbf{f}}_p(\hat{\mathbf{r}}, \hat{t}) = \phi\mathbf{f}_p(\mathbf{r}, t) \quad (15)$$

In the oblique coordinate system, $\hat{\mathbf{u}}$ satisfies the standard periodic boundary conditions while \mathbf{u} satisfies the Lees-Edwards periodic boundary conditions in the rectangular coordinate system. The contravariant components $(\hat{u}^1, \hat{u}^2, \hat{u}^3)$ of $\hat{\mathbf{u}}$ are expressed as

$$\begin{aligned} \hat{u}^1 &= u_x - \dot{\gamma}t u_y - \dot{\gamma}y \\ \hat{u}^2 &= u_y \\ \hat{u}^3 &= u_z \end{aligned} \quad (16)$$

where (u_x, u_y, u_z) are the rectangular components of \mathbf{u} . The contravariant components of $\hat{\phi}\hat{\mathbf{f}}_p$ are $(\hat{\phi}\hat{f}_p^1, \hat{\phi}\hat{f}_p^2, \hat{\phi}\hat{f}_p^3)$ and can be expressed as

$$\begin{aligned} \hat{\phi}\hat{f}_p^1 &= \phi f_p^x - \dot{\gamma}t \phi f_p^y \\ \hat{\phi}\hat{f}_p^2 &= \phi f_p^y \\ \hat{\phi}\hat{f}_p^3 &= \phi f_p^z \end{aligned} \quad (17)$$

where (f_p^x, f_p^y, f_p^z) are the rectangular components of \mathbf{f}_p .

The differential operators in oblique coordinates are defined by

$$\hat{\nabla} = \hat{\mathbf{E}}^1 \frac{\partial}{\partial \hat{x}^1} + \hat{\mathbf{E}}^2 \frac{\partial}{\partial \hat{x}^2} + \hat{\mathbf{E}}^3 \frac{\partial}{\partial \hat{x}^3} \quad (18)$$

$$\frac{\partial}{\partial \hat{t}} = \frac{\partial}{\partial t} + \dot{\gamma}y \frac{\partial}{\partial x} \quad (19)$$

Therefore, the Laplacian operator in oblique coordinates is expressed as

$$\hat{\Delta} = \left(\frac{\partial}{\partial \hat{x}^1} \right)^2 + \left(\frac{\partial}{\partial \hat{x}^2} - \dot{\gamma}t \frac{\partial}{\partial \hat{x}^1} \right)^2 + \left(\frac{\partial}{\partial \hat{x}^3} \right)^2 \quad (20)$$

Using these formula, Eqs. (1) and (2) are rewritten in oblique coordinates as

$$\begin{aligned} \rho \left\{ \frac{\partial \hat{\mathbf{u}}}{\partial \hat{t}} + (\hat{\mathbf{u}} \cdot \hat{\nabla}) \hat{\mathbf{u}} \right\} \\ = \hat{\nabla} \cdot \hat{\boldsymbol{\sigma}} + \rho \hat{\phi} \hat{\mathbf{f}}_p - \rho \dot{\gamma} \hat{u}^2 \hat{\mathbf{E}}_1 - K \rho (\hat{u}^1 + \gamma \hat{u}^2) \hat{\mathbf{E}}_1 \end{aligned} \quad (21)$$

and

$$\hat{\sigma}^{ij}(\hat{\mathbf{r}}, \hat{t}) = -G^{ij} \hat{p}(\hat{\mathbf{r}}, \hat{t}) + \eta_f \left\{ G^{in} \frac{\partial \hat{u}^j}{\partial \hat{x}^n} + G^{jm} \frac{\partial \hat{u}^i}{\partial \hat{x}^m} \right\} \quad (22)$$

with the incompressibility condition $\hat{\nabla} \cdot \hat{\mathbf{u}} = 0$. Because Eq. (21) and $\hat{\mathbf{u}}$ satisfy the periodic boundary conditions in all directions, a fast Fourier transformation (FFT) can be safely used

to solve the Poisson equation, which is needed to determine \hat{p} with the incompressibility condition. In Appendix 1, detailed explanations are given on how to solve Eq. (21) with the incompressibility condition in the oblique coordinate system with using the spectral (Fourier) method.

When $\gamma \equiv \dot{\gamma}t = 1$, the positions $\hat{\mathbf{r}} = (\hat{x}^1, \hat{x}^2, \hat{x}^3)$ on an oblique grid with γ can be mapped onto the identical positions $\mathbf{r} = (x, y, z)$ on the original rectangular grid with $\gamma = 0$ using the operation $x = \hat{x}^1 + \hat{x}^2$, $y = \hat{x}^2$, $z = \hat{x}^3$. The shear strain γ is then reset to 0.⁶ Repeating this process allows us to perform stable numerical calculations over a long period with keeping $0 \leq \gamma \leq 1$. The above coordinate transformation based on the tensor analysis leads to the same expression for the Laplacian $\hat{\Delta}$ as that of a previous study.⁶ However, a difference arises between the differential operators $\hat{\nabla}$ for which our formal transformation derives a much simpler expression as shown in Eq. (18).

We calculate the dynamics of solid particle dispersions in shear flow by following these steps:

i) The fluid velocity field in the oblique coordinate system at a new time $t = nh$ is calculated by integrating Eq. (21) over time with $\hat{\phi}\hat{\mathbf{f}}_p = 0$ as

$$\hat{\mathbf{u}}^* = \hat{\mathbf{u}}^{n-1} + \int_{t_{n-1}}^{t_{n-1}+h} \left[\hat{\nabla} \cdot \left(\frac{1}{\rho} \hat{\boldsymbol{\sigma}} - \hat{\mathbf{u}}\hat{\mathbf{u}} \right) - \{K(\hat{u}^1 + \gamma\hat{u}^2) + 2\dot{\gamma}\hat{u}^2\} \hat{\mathbf{E}}_1 \right] ds \quad (23)$$

while satisfying the incompressibility condition $\hat{\nabla} \cdot \hat{\mathbf{u}}^* = 0$. Here, the superscript n denotes the time step, and h is the time increment. In Appendix 1, detailed explanations are given also on how to solve Eq. (23) with using the spectral method.

ii) The velocity field $\hat{\mathbf{u}}^*$ is transformed into rectangular coordinates \mathbf{u}^* using the inverse transformation expressed as

$$\begin{aligned} u_x &= \hat{u}^1 + \dot{\gamma}t\hat{u}^2 + \dot{\gamma}\hat{x}^2 \\ u_y &= \hat{u}^2 \\ u_z &= \hat{u}^3. \end{aligned} \quad (24)$$

iii) The motions of colloidal particles are only calculated in rectangular coordinates. The position of each colloidal particle is calculated by

$$\mathbf{r}_i^n = \mathbf{r}_i^{n-1} + \int_{t_{n-1}}^{t_{n-1}+h} \mathbf{v}_i^{n-1} ds \quad (25)$$

iv) Using the momentum conservation between colloidal particles and the solvent, the hydrodynamic force and torque acting on each colloidal particle are computed with volume integrals within the particle domain as

$$\mathbf{f}_i^H = \frac{\rho}{h} \int d\mathbf{r} [\phi_i^n (\mathbf{u}^* - \mathbf{u}_p^{n-1})] \quad (26)$$

and

$$\mathbf{n}_i^H = \frac{\rho}{h} \int d\mathbf{r} [(\mathbf{r} - \mathbf{r}_i) \times \phi_i^n (\mathbf{u}^* - \mathbf{u}_p^{n-1})] \quad (27)$$

where $\phi \mathbf{u}_p^{n-1}(\mathbf{r}) = \sum_i \phi_i^n(\mathbf{r}) (\mathbf{v}_i^{n-1} + \boldsymbol{\omega}_i^{n-1} \times (\mathbf{r} - \mathbf{r}_i))$ is the correct velocity field within the particle domain in which $\phi \simeq 1$. The space integrals in Eqs.(26) and (27) are carried out by summations over grid points in actual computations, however, there occur grid mismatch between \mathbf{u}^* which is supported on oblique grid points $\hat{\mathbf{r}}_{i,\hat{j},\hat{k}}$ and other variables (ϕ_i^n and $\phi \mathbf{u}_p^{n-1}$) which are supported on rectangular grid points $\mathbf{r}_{i,j,k}$. We determine values of \mathbf{u}^* on rectangular grid points $\mathbf{r}_{i,j,k}$ by linear interpolation as described in detail in Appendix 2. The translational velocity and rotational velocity of each colloidal particle are then calculated as

$$\mathbf{v}_i^n = \mathbf{v}_i^{n-1} + \frac{1}{M_i} \int_{t_{n-1}}^{t_{n-1}+h} (\mathbf{f}_i^H + \mathbf{f}_i^P + \mathbf{g}_i^V) ds \quad (28)$$

and

$$\boldsymbol{\omega}_i^n = \boldsymbol{\omega}_i^{n-1} + \mathbf{I}_i^{-1} \int_{t_{n-1}}^{t_{n-1}+h} (\mathbf{n}_i^H + \mathbf{g}_i^\omega) ds \quad (29)$$

v) To ensure the rigidity of the particles and the appropriate non-slip boundary conditions at the fluid/particle interface, the body force $\phi \mathbf{f}_p$ is calculated as

$$\phi \mathbf{f}_p = \frac{\phi (\mathbf{u}_p^n - \mathbf{u}^*)}{h} - \frac{1}{\rho} \nabla p_p. \quad (30)$$

The correcting pressure p_p is determined to make the resultant total velocity incompressible. This leads to the Poisson equation of p_p :

$$\Delta p_p = \rho \frac{\nabla \cdot \phi (\mathbf{u}_p^n - \mathbf{u}^*)}{h}. \quad (31)$$

We then transform $\phi \mathbf{f}_p$ into oblique coordinates $\hat{\phi} \hat{\mathbf{f}}_p$ using Eqs. (15) and (17).

vi) Finally, we obtain the correct fluid velocity field as:

$$\hat{\mathbf{u}}^n = \hat{\mathbf{u}}^* + \hat{\phi} \hat{\mathbf{f}}_p h. \quad (32)$$

Repetition of steps i) through vi) provides a complete procedure to perform the DNS of colloidal dispersions under shear flow.

We can calculate the stress tensor of the dispersion $\langle \mathbf{s} \rangle$ and the dispersion viscosity $\eta = \langle s_{xy} \rangle / \dot{\gamma}$ in the following manner where $\langle \dots \rangle$ denotes averaging over space and time. The equation governing the dispersion is formally written as:

$$\frac{D}{Dt}(\rho \mathbf{u}) = \nabla \cdot \boldsymbol{\sigma}^{\text{dis}} - K\rho(u_x - \dot{\gamma}y)\mathbf{e}_x \quad (33)$$

By comparing Eq. (1) with Eq. (33), we get the formula

$$\nabla \cdot \boldsymbol{\sigma}^{\text{dis}} = \nabla \cdot \boldsymbol{\sigma} + \rho\phi \mathbf{f}_p. \quad (34)$$

The full stress tensor \mathbf{s} of the flowing dispersion is then defined by introducing a convective momentum-flux tensor explicitly as

$$\mathbf{s} = \boldsymbol{\sigma}^{\text{dis}} - \rho \mathbf{u} \mathbf{u}. \quad (35)$$

The definitions of $\boldsymbol{\sigma}^{\text{dis}}$ and \mathbf{s} are identical to the definitions in our previous paper.⁴ Now, we can evaluate the average stress tensor of the dispersion $\langle \mathbf{s} \rangle$ directly from Eqs. (34), (35), and $\delta \boldsymbol{\sigma} = \mathbf{s} - \boldsymbol{\sigma}$ as

$$\begin{aligned} \langle \mathbf{s} \rangle &= \langle \boldsymbol{\sigma} \rangle + \frac{1}{V} \left\langle \int \mathbf{dr} \delta \boldsymbol{\sigma} \right\rangle_t \\ &= \langle \boldsymbol{\sigma} \rangle + \frac{1}{V} \left\langle \int \mathbf{dr} \left[(\nabla \cdot (\delta \boldsymbol{\sigma} \mathbf{r}))^T - \mathbf{r} \nabla \cdot \delta \boldsymbol{\sigma} \right] \right\rangle_t \\ &= \langle \boldsymbol{\sigma} \rangle - \frac{1}{V} \left\langle \int \mathbf{dr} \mathbf{r} \nabla \cdot \delta \boldsymbol{\sigma} \right\rangle_t \\ &= \langle \boldsymbol{\sigma} \rangle - \frac{1}{V} \left\langle \int \mathbf{dr} \mathbf{r} \rho \phi \mathbf{f}_p \right\rangle_t + \frac{1}{V} \left\langle \int \mathbf{dr} \mathbf{r} \mathbf{u} \cdot \nabla (\rho \mathbf{u}) \right\rangle_t \\ &= \langle \boldsymbol{\sigma} \rangle - \frac{1}{V} \left\langle \int \mathbf{dr} \mathbf{r} \rho \phi \mathbf{f}_p \right\rangle_t \end{aligned} \quad (36)$$

with the volume $V = L_x L_y L_z$ where L_i is the system size in i -direction. $\langle \dots \rangle_t$ denotes time averaging over steady state. In the derivation of the second formula, we used a second rank identity. If we substitute Eq. (34) into the third formula, then we obtain the fourth formula. The fifth formula can be obtained by assuming that the system is in a steady state in which $\langle \frac{d}{dt}(\rho \mathbf{u}) \rangle_t = \langle \frac{\partial}{\partial t}(\rho \mathbf{u}) + \mathbf{u} \cdot \nabla(\rho \mathbf{u}) \rangle_t = 0$ and $\langle \frac{\partial}{\partial t}(\rho \mathbf{u}) \rangle_t = 0$.

III. RESULTS

Using the method described above, we calculated the high- and low-shear limiting viscosities of colloidal dispersions for various volume fractions of particles Φ . The particles interact via a truncated Mie (m, n) potential with $m = 36$ and $n = 18$.¹³

$$U(r) = \begin{cases} 4\epsilon \left\{ \left(\frac{\sigma}{r}\right)^{36} - \left(\frac{\sigma}{r}\right)^{18} \right\} + \epsilon & (r < 2^{\frac{1}{18}}\sigma), \\ 0 & (r > 2^{\frac{1}{18}}\sigma), \end{cases} \quad (37)$$

where r is the distance between the centers of a pair of particles. The parameter ϵ characterizes the strength of the interactions, and σ represents the diameter of the colloidal particles. The lattice spacing δx is taken to be the unit of length. The unit of time is given by $\rho_f \delta x^2 / \eta$ where $\eta = 1$ and $\rho_f = \rho_p = 1$. The system size is $L_x \times L_y \times L_z = 64 \times 64 \times 64$. Other parameters are set as follows: $\sigma = 8$, $\xi = 2$, $\epsilon = 1$, $\eta = 1$, $M_i = \pi\sigma^3/6$, and $h = 0.067$. The temperature is $k_B T = 7$. The range of shear rate is $1.0 \times 10^{-4} < \dot{\gamma} < 0.1$.

The inset of Fig. 3 shows the dependence of the Newtonian viscosity on the volume fraction Φ when $\Phi \ll 1$. The present simulation data show very good agreement with Einstein's viscosity law. Fig. 3 shows the dependence of the low-shear limiting viscosity (closed symbols) and the high-shear limiting viscosity (open symbols) on the volume fraction. Our simulation data for both high- and low-shear limiting viscosities show good agreement with the experimental results of van der Werff *et al.*¹⁴ Previously, Brady theoretically predicted the behavior of the low-shear limiting viscosity.¹⁵ Our simulation data show good agreement with Brady's prediction over a wide range of volume fractions $0 < \Phi < 0.55$. Ladd analyzed the behavior of the high-shear limiting viscosity using Stokesian dynamics.¹⁶ Our simulation data agree well with Ladd's simulation data and also with the theoretical results of Beenakker.¹⁷

Finally, we add some comments on the differences between the present method using Lees-Edwards boundary condition and the previously proposed method using zigzag velocity profile.¹⁸ We simulated a single spherical particle in shear flow using the two methods without thermal fluctuation. The volume fraction is 0.001. Figure 5 shows the ratio of angular velocity ω of a spherical particle to the applied shear rate $\dot{\gamma}$ as a function of $\dot{\gamma}$. Although the data using the present method tend to be slightly smaller than the data using the zigzag flow, deviations of both data from the analytical value $\omega/\dot{\gamma} = 0.5$ remain small within numerical errors of the methods. Figure 6 shows the intrinsic viscosity $[\eta]$ of the dilute dispersion as

a function of shear rate $\dot{\gamma}$. The simulation data using the present method almost perfectly follow onto the Einstein's prediction $[\eta] = 2.5$, while the data using zigzag flow slightly overestimate $[\eta]$ because of unphysical kinks of the zigzag flow profile. This problem is not very serious when the shape of dispersed particles is spherical and the size of the particle is much smaller than the distance between two kinks. Serious problems, however, occur if this method is applied to non-dilute dispersions of chains or rods, for example. The present method using Lees-Edwards boundary condition is free from this problem.

IV. CONCLUSION

We presented a generic methodology for performing DNS of particle dispersions in a shear flow using oblique coordinates and periodic boundary conditions. The validity of the method was confirmed by comparing the present numerical results with experimental viscosity data for particle dispersions over a wide range of the parameters Φ and $\dot{\gamma}$ that include nonlinear shear-thinning regimes. An important advantage of the DNS approach over other approaches such as Stokesian dynamics is its applicability to particle dispersions in complex fluids. In fact, electrophoresis of charged colloids¹⁹ and particle dispersions in nematic liquid crystals²⁰ have already been calculated using SPM. Our methodology can also be applied to simulate particle dispersions in viscoelastic fluids simply by replacing the Newtonian constitutive equation to more complex ones such as Maxwell model.

ACKNOWLEDGMENTS

The authors would like to express their gratitude to Dr. T. Murashima, Dr. Y. Nakayama, Dr. K. Kim, and Dr. T. Iwashita for useful comments and discussions.

APPENDIX 1

In this section, we describe how to solve Eq. (21) with the incompressibility condition in an oblique coordinate system using Fourier spectral methods. The Fourier and inverse Fourier transforms are defined as

$$A(\hat{\mathbf{k}}) = \int A(\hat{\mathbf{r}}) \exp(-i\hat{\mathbf{k}} \cdot \hat{\mathbf{r}}) d\hat{\mathbf{r}} \quad (38)$$

$$A(\hat{\mathbf{r}}) = \frac{1}{(2\pi)^3} \int A(\hat{\mathbf{k}}) \exp(i\hat{\mathbf{k}} \cdot \hat{\mathbf{r}}) d\hat{\mathbf{k}}, \quad (39)$$

where $\hat{\mathbf{k}}$ is the wavevector of the oblique coordinate system. In $\hat{\mathbf{k}}$ space, we can express the spatial covariant derivative as

$$\frac{\partial A(\hat{\mathbf{r}})}{\partial x^{\hat{\alpha}}} \rightarrow ik_{\alpha} A(\hat{\mathbf{k}}). \quad (40)$$

where k_{α} is a covariant component of $\hat{\mathbf{k}}$.

Using these relations, we modify Eq. (23) from $\hat{\mathbf{r}}$ space to $\hat{\mathbf{k}}$ space. This equation is solved in $\hat{\mathbf{k}}$ space. First, by substituting Eq. (22) into Eq. (23), we obtain the explicit equation represented by

$$\hat{\mathbf{u}}^*(\hat{\mathbf{r}}) = \hat{\mathbf{u}}(\hat{\mathbf{r}}) + \int_{t_{n-1}}^{t_{n-1}+h} \left[-(\hat{\mathbf{u}}(\hat{\mathbf{r}}) \cdot \hat{\nabla}) \hat{\mathbf{u}}(\hat{\mathbf{r}}) - \hat{\nabla} \frac{\hat{p}(\hat{\mathbf{r}})}{\rho} + \nu \hat{\Delta} \hat{\mathbf{u}}(\hat{\mathbf{r}}) - \{K(\hat{u}^1(\hat{\mathbf{r}}) + \gamma \hat{u}^2(\hat{\mathbf{r}})) + 2\dot{\gamma} \hat{u}^2(\hat{\mathbf{r}})\} \hat{\mathbf{E}}_1 \right] ds, \quad (41)$$

where $\nu = \eta_f/\rho$ is the kinetic viscosity. Using a Fourier transform, the form of Eq. (41) in $\hat{\mathbf{k}}$ space is written as

$$\hat{\mathbf{u}}^*(\hat{\mathbf{k}}) = \hat{\mathbf{u}}(\hat{\mathbf{k}}) + \int_{t_{n-1}}^{t_{n-1}+h} \left[-\mathbf{F}(\hat{\mathbf{k}}) - \nu \hat{\mathbf{k}}^2 \hat{\mathbf{u}}(\hat{\mathbf{k}}) - \{K(\hat{u}^1(\hat{\mathbf{k}}) + \gamma \hat{u}^2(\hat{\mathbf{k}})) + 2\dot{\gamma} \hat{u}^2(\hat{\mathbf{k}})\} \hat{\mathbf{E}}_1 \right]_{\perp} ds, \quad (42)$$

where

$$\mathbf{F}(\hat{\mathbf{k}}) = \int (\hat{\mathbf{u}}(\hat{\mathbf{r}}) \cdot \hat{\nabla}) \hat{\mathbf{u}}(\hat{\mathbf{r}}) \exp(-i\hat{\mathbf{k}} \cdot \hat{\mathbf{r}}) d\hat{\mathbf{r}}. \quad (43)$$

The bracket $\left[\mathbf{A}(\hat{\mathbf{k}}) \right]_{\perp} \left(\equiv \mathbf{A}(\hat{\mathbf{k}}) \cdot \left(\mathbf{I} - \frac{\hat{\mathbf{k}}\hat{\mathbf{k}}}{\hat{\mathbf{k}}^2} \right) \right)$ denotes taking the orthogonal part to $\hat{\mathbf{k}}$ and this operation corresponds to imposing the incompressibility condition $\hat{\nabla} \cdot \hat{\mathbf{u}}(\hat{\mathbf{r}}) = 0$ (or equivalently $\hat{\mathbf{k}} \cdot \hat{\mathbf{u}}(\hat{\mathbf{k}}) = 0$). Because $\hat{p}(\hat{\mathbf{r}})$ is automatically determined by imposing the condition of incompressibility, we can safely neglect this term.

Using the method describe above, we calculate $\hat{\mathbf{u}}^*(\hat{\mathbf{r}})$ from $\hat{\mathbf{u}}(\hat{\mathbf{r}})$ as shown in Eq. (23).

APPENDIX 2

An arbitrary position vector in the oblique coordinate system is defined as

$$\hat{\mathbf{r}}_{\hat{i},\hat{j},\hat{k}} = (\hat{i}\hat{\mathbf{E}}_1 + \hat{j}\hat{\mathbf{E}}_2 + \hat{k}\hat{\mathbf{E}}_3)\delta x \quad (44)$$

with arbitrary integer numbers $\hat{i}, \hat{j}, \hat{k}$, while a position vector in the rectangular coordinate system is defined as

$$\mathbf{r}_{i,j,k} = (ie_x + je_x + ke_x)\delta x \quad (45)$$

with integer numbers i, j, k , where δx represents the lattice spacing. In general, the two position vectors $\hat{\mathbf{r}}_{\hat{i},\hat{j},\hat{k}}$ and $\mathbf{r}_{i,j,k}$ are not compatible with each other. To transform from $\hat{\mathbf{r}}_{\hat{i},\hat{j},\hat{k}}$ to $\mathbf{r}_{i,j,k}$ using Eq. (9), i must equal $\hat{i} - \gamma\hat{j}$. However, $\gamma\hat{j}$ is not always an integer since γ is defined between 0 and 1. We thus perform interpolation of the variables to overcome this problem.

Fig. 4 shows a lattice discordance between the rectangular and oblique coordinate systems. $\mathbf{r}_{i,j,k}$ is the location vector in rectangular coordinates, and $\hat{\mathbf{r}}_{\hat{i}-1,\hat{j},\hat{k}}$ and $\hat{\mathbf{r}}_{\hat{i},\hat{j},\hat{k}}$ are the location vectors in oblique coordinates. Using liner interpolation, we estimate the velocity field in rectangular coordinates $\mathbf{u}(\mathbf{r}_{i,j,k})$ from the velocity field in oblique coordinates $\mathbf{u}(\hat{\mathbf{r}}_{\hat{i}-1,\hat{j},\hat{k}})$ and $\mathbf{u}(\hat{\mathbf{r}}_{\hat{i},\hat{j},\hat{k}})$. From the liner interpolation, $\mathbf{u}(\mathbf{r}_{i,j,k})$ along the straight line is given by the equation

$$\mathbf{u}(\mathbf{r}_{i,j,k}) = \frac{|\hat{\mathbf{r}}_{\hat{i},\hat{j},\hat{k}} - \mathbf{r}_{i,j,k}|}{|\hat{\mathbf{r}}_{\hat{i},\hat{j},\hat{k}} - \hat{\mathbf{r}}_{\hat{i}-1,\hat{j},\hat{k}}|} \mathbf{u}(\hat{\mathbf{r}}_{\hat{i}-1,\hat{j},\hat{k}}) + \frac{|\hat{\mathbf{r}}_{\hat{i}-1,\hat{j},\hat{k}} - \mathbf{r}_{i,j,k}|}{|\hat{\mathbf{r}}_{\hat{i},\hat{j},\hat{k}} - \hat{\mathbf{r}}_{\hat{i}-1,\hat{j},\hat{k}}|} \mathbf{u}(\hat{\mathbf{r}}_{\hat{i},\hat{j},\hat{k}}). \quad (46)$$

When using liner interpolation, artificial diffusion may arise. To check the reliability of the present method, we calculate the angular velocity ω and intrinsic viscosity $[\eta] = \lim_{\Phi \rightarrow 0} (\eta - \eta_f)/\Phi$ for a dilute dispersion of spherical particle for which analytical solutions are available. As already shown in Figs. 5 and 6, the present simulation data agree very well with analytical solutions indicating that the effects of artificial numerical diffusion are not serious.

REFERENCES

- ¹Y. Nakayama and R. Yamamoto, Phys. Rev. E **71**, 036707 (2005).
- ²Y. Nakayama, K. Kim, and R. Yamamoto, Eur. Phys. J. E **26**, 361 (2008).

- ³T. Iwashita, Y. Nakayama, and R. Yamamoto, *J. Phys. Soc. Jpn.* **77** 074007 (2008).
- ⁴T. Iwashita and R. Yamamoto, *Phys. Rev. E* **79** 031401 (2009).
- ⁵A. W. Lees and S. F. Edwards, *J. Phys. C* **5**, 1921 (1972).
- ⁶A. Onuki, *J. Phys. Soc. Jpn.* **66**, 1836 (1997).
- ⁷S. Toh, K. Ohkitani, and M. Yamada, *Physica D* **51**, 569 (1991).
- ⁸R. S. Rogallo, NASA Tech. Mem., 81315 (1981).
- ⁹A. Onuki, R. Yamamoto, and T. Taniguchi, *J. Phys. II France* **7**, 295 (1997).
- ¹⁰Z. Zhang, H. Zhang, and Y. Yang, *J. Chem. Phys.* **115**, 7783 (2001).
- ¹¹T. Imaeda, A. Furukawa, A. Onuki, *Phys. Rev. E* **70**, 051503 (2004).
- ¹²S. Nishitsuji, M. Takenaka, T. Taniguchi, *Polymer* **51**, 1853 (2010).
- ¹³G. Mie, *Annalen der Physik* **11**, 657 (1903).
- ¹⁴J. C. van der Werff, C. G. de Kruif, C. Blom, and J. Mellema, *Phys. Rev. A* **39**, 795 (1989).
- ¹⁵J. F. Brady, *J. Chem. Phys.* **99**, 567 (1993).
- ¹⁶A. J. C. Ladd, *J. Chem. Phys.* **93**, 3484 (1990).
- ¹⁷C. W. J. Beenakker, *Physica A* **128**, 48 (1984).
- ¹⁸T. Iwashita, R. Yamamoto, *Phys. Rev. E* **80**, 061402 (2009).
- ¹⁹K. Kim, Y. Nakayama, R. Yamamoto, *Phys. Rev. Lett.* **96**, 208302 (2006).
- ²⁰R. Yamamoto, *Phys. Rev. Lett.* **87**, 075502 (2001).

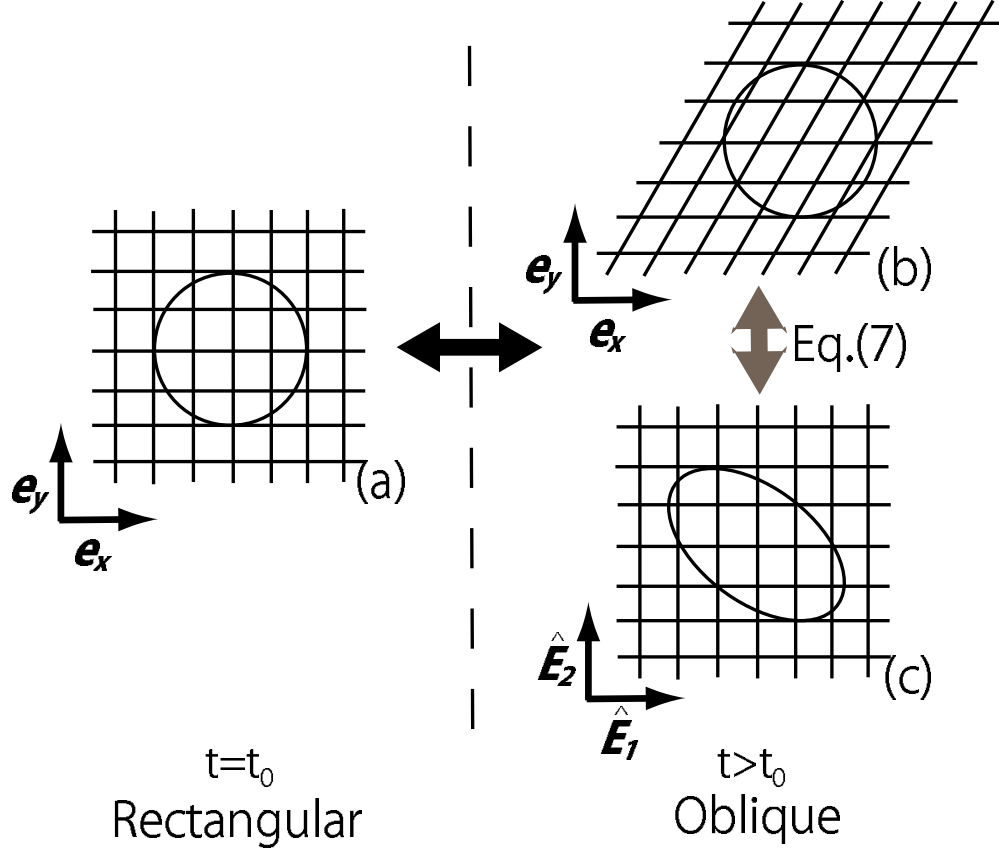


FIG. 1. A schematic illustration of the present coordinate transformation. In (a), a spherical solid particle is in a solvent, which is discretized into grids in an ordinary rectangular coordinate system, at a time $t = t_0$. Since the shear flow is applied for $t > t_0$, the solvent (grids) is convected by the flow while the shape of the solid particle is unchanged. Such a situation is depicted in the original (experimental) frame in (b) and also in a transformed (oblique) frame in (c). The transformation between (b) and (c) is defined by Eq. (7).

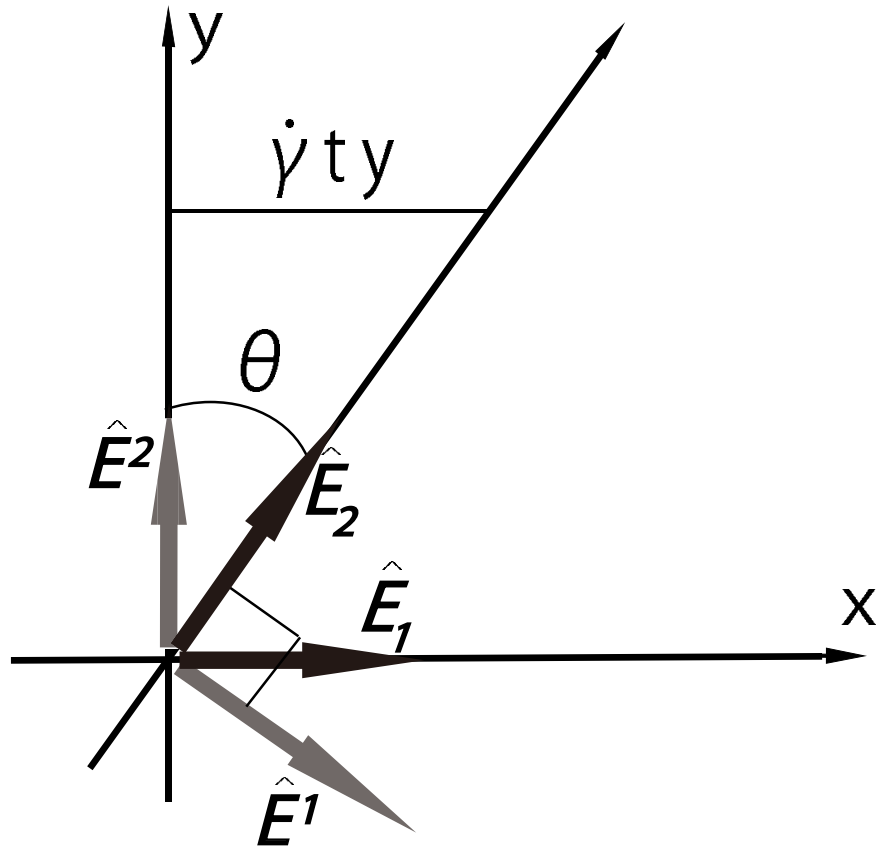


FIG. 2. The definition of a basis vector.

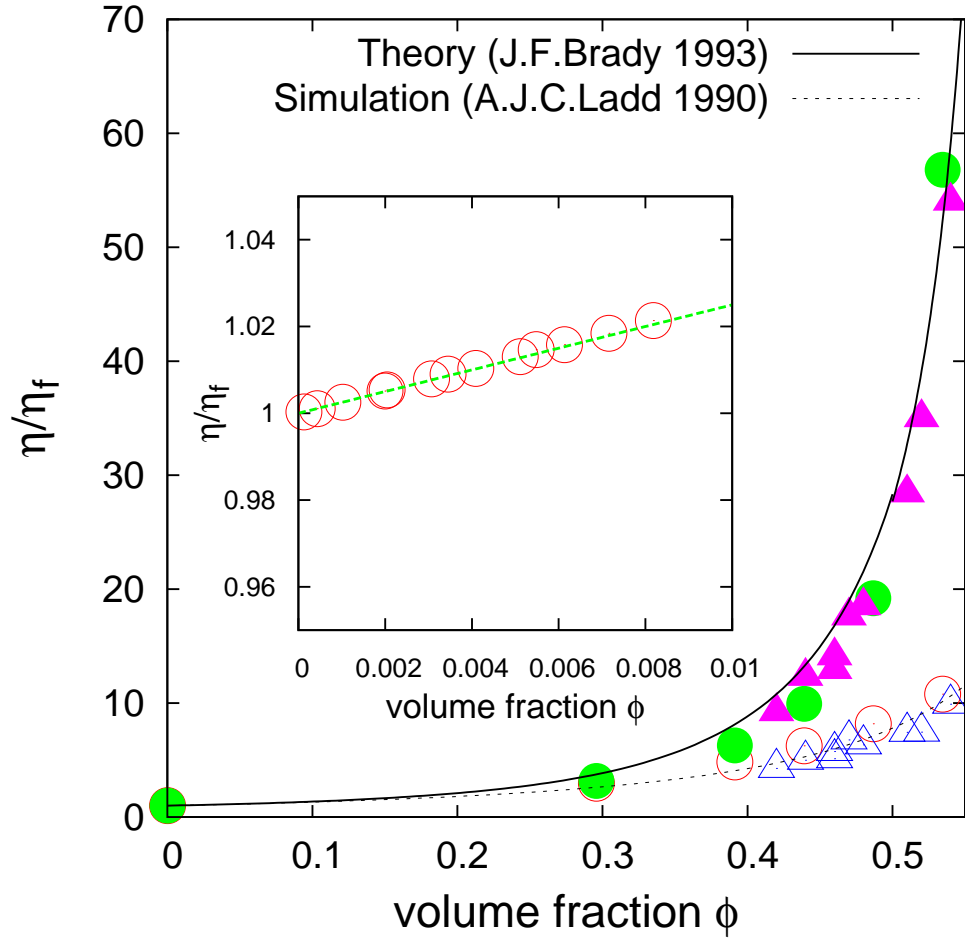


FIG. 3. The behavior of the viscosity η as a function of the volume fraction Φ . The open symbols represent the high-shear limiting viscosity, and the closed symbols represent the low-shear limiting viscosity. The open and closed circles correspond to our simulation data, whereas the triangles correspond to experimental results.¹⁴ The solid line is Brady's theoretical prediction,¹⁵ and the dotted line is a fitting curve obtained from previous experimental¹⁴ and simulation¹⁶ data. The inset indicates a comparison of our present simulation data with Einstein's viscosity law (dashed-line) in the small volume fraction regime $\Phi < 0.01$ where the viscosity exhibits simple Newtonian behavior.

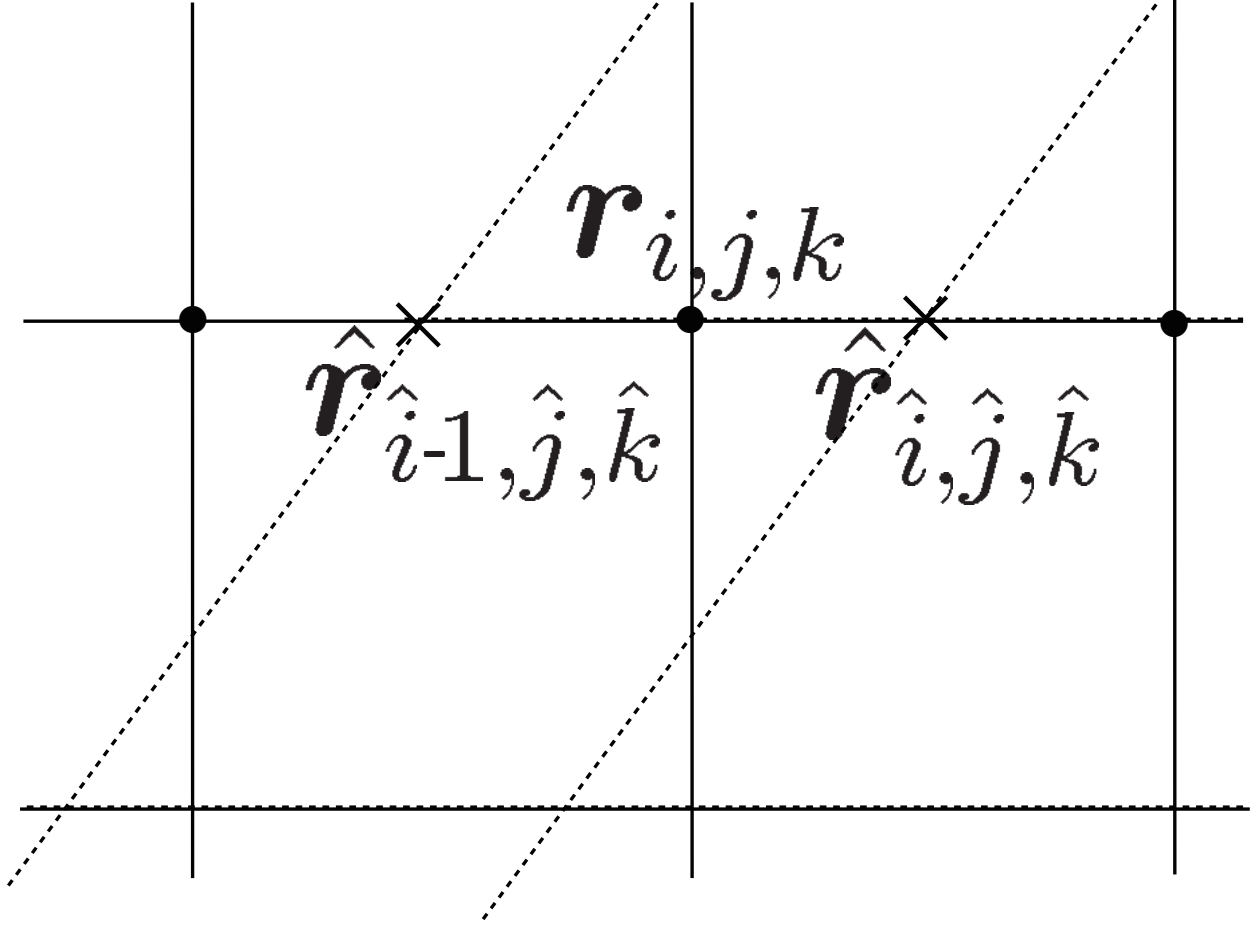


FIG. 4. A schematic illustration of the lattice discordance between the oblique and rectangular coordinates. $\mathbf{r}_{i,j,k}$ is the location vector in a rectangular coordinate system. $\hat{\mathbf{r}}_{\hat{i}-1, \hat{j}, \hat{k}}$ and $\hat{\mathbf{r}}_{\hat{i}, \hat{j}, \hat{k}}$ are the location vectors in the oblique coordinate system.

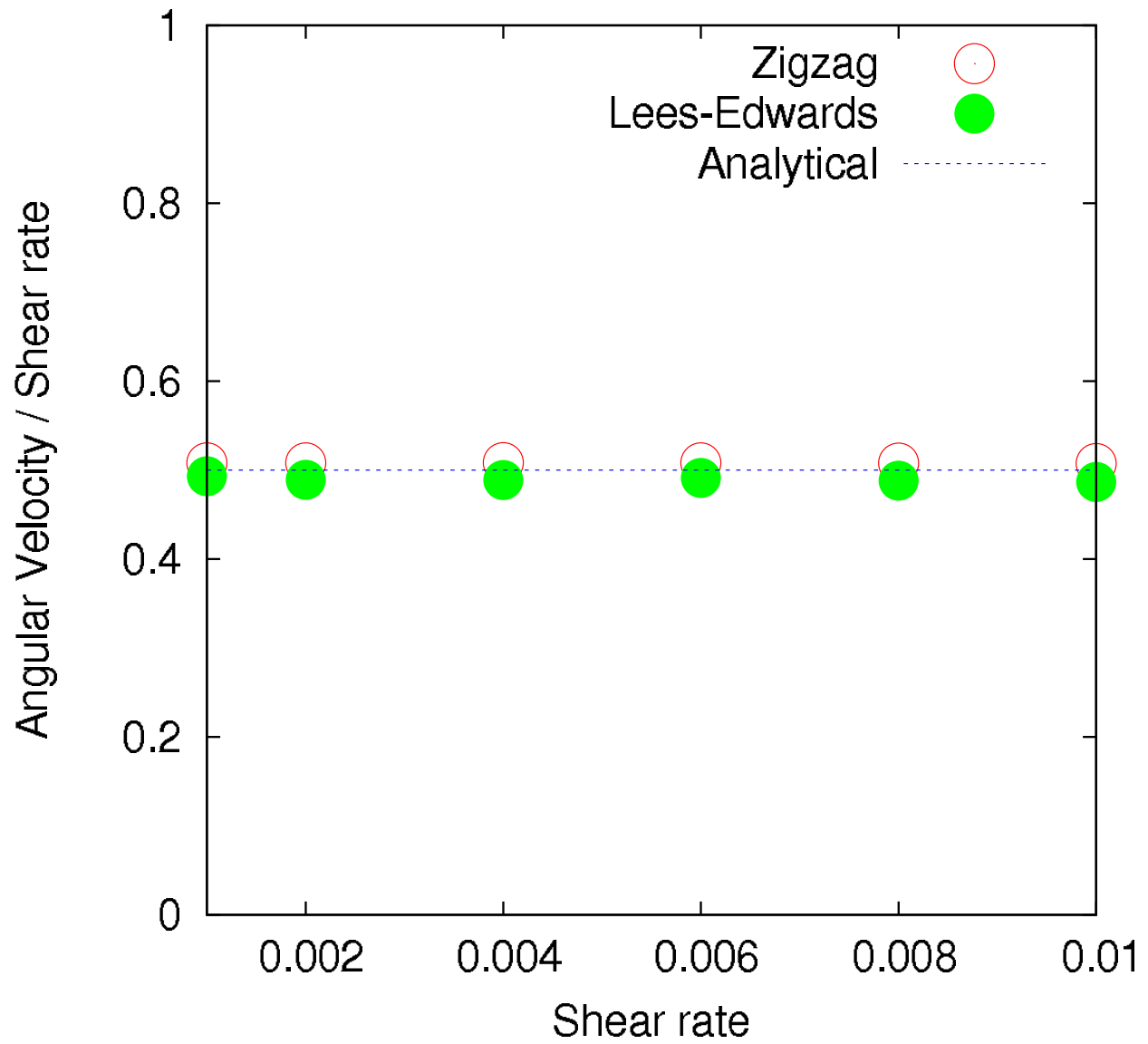


FIG. 5. The behavior of the ratio of angular velocity ω to the shear rate $\dot{\gamma}$ as a function of $\dot{\gamma}$. Open circles indicate the results of the previous method. Closed circles indicate the results of the present method. The solid line corresponds to the analytical solution.

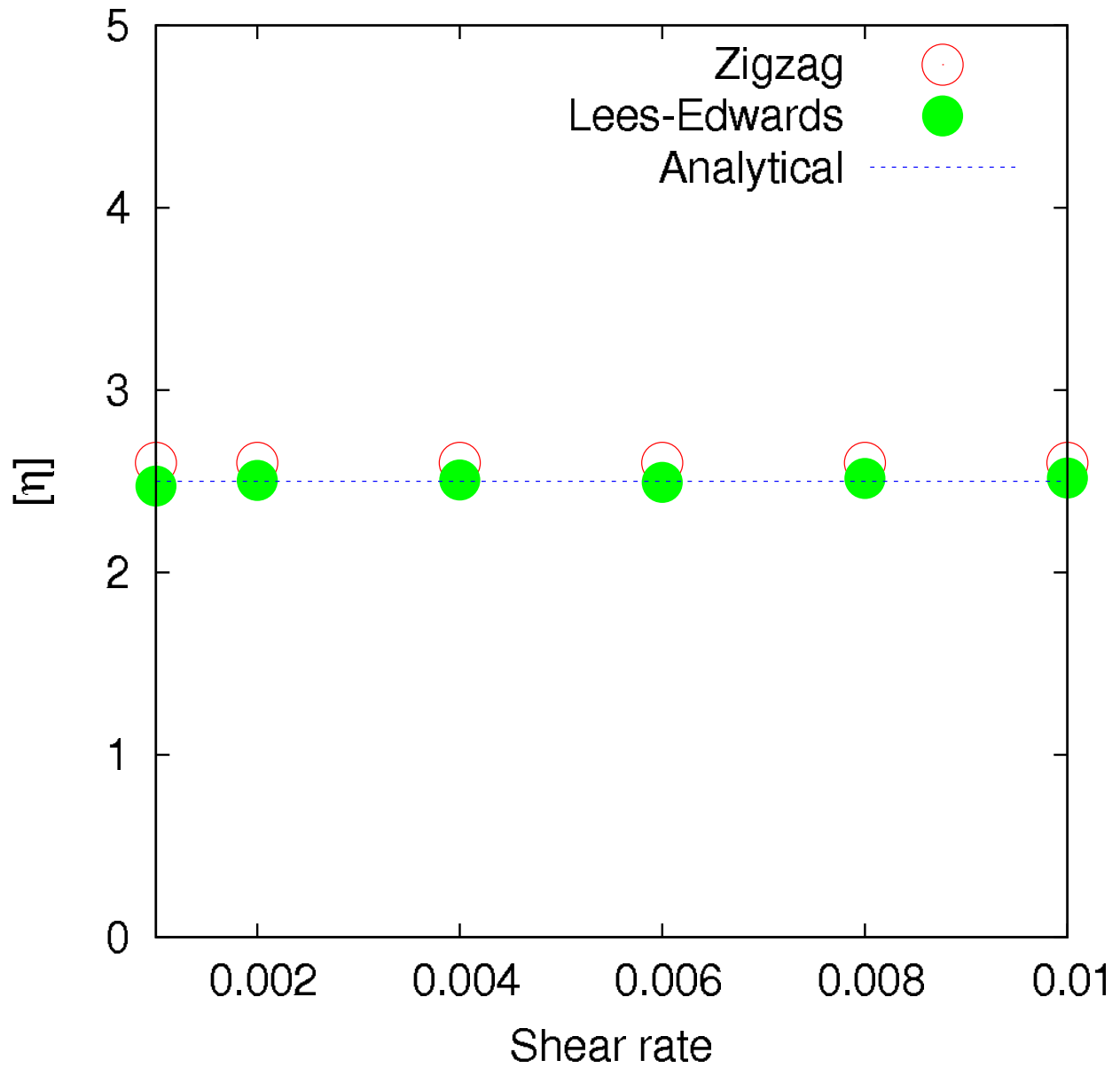


FIG. 6. The behavior of the intrinsic viscosity as a function of shear rate $\dot{\gamma}$. Open circles indicate the results of the previous method. Closed circles indicate the results of the present method. The solid line corresponds to Einstein's viscosity law.